CHINESE JOURNAL OF MECHANICAL ENGINEERING
Vol. 27, No. 3, 2014

DOI: 10.3901/CJME.2014.03.558, available online at www.springerlink.com; www.cjmenet.com; www.cjmenet.com.cn

Theoretical and Experimental Research on Error Analysis and Optimization of Tool Path in Fabricating Aspheric Compound Eyes by Precision Micro Milling

CHEN Mingjun*, XIAO Yong, TIAN Wenlan, WU Chunya, and CHU Xin

Center for Precision Engineering, Harbin Institute of Technology, Harbin 150001, China

Received July 13, 2013; revised February 17, 2014; accepted March 25, 2014

Abstract: Structure design and fabricating methods of three-dimensional (3D) artificial spherical compound eyes have been researched by many scholars. Micro-nano optical manufacturing is mostly used to process 3D artificial compound eyes. However, spherical optical compound eyes are less at optical performance than the eyes of insects, and it is difficult to further improve the imaging quality of compound eyes by means of micro-nano optical manufacturing. In this research, nonhomogeneous aspheric compound eyes (ACEs) are designed and fabricated. The nonhomogeneous aspheric structure is applied to calibrate the spherical aberration. Micro milling with advantages in processing three-dimensional micro structures is adopted to manufacture ACEs. In order to obtain ACEs with high imaging quality, the tool paths are optimized by analyzing the influence factors consisting of interpolation allowable error, scallop height and tool path pattern. In the experiments, two kinds of ACEs are manufactured by micro-milling with different too path patterns and cutting parameter on the miniature precision five-axis milling machine tool. The experimental results indicate that the ACEs of high surface quality can be achieved by circularly milling small micro-lens individually with changeable cutting depth. A prototype of the aspheric compound eye (ACE) with surface roughness (R_a) below 0.12 μm is obtained with good imaging performance. This research ameliorates the imaging quality of 3D artificial compound eyes, and the proposed method of micro-milling can improve surface processing quality of compound eyes.

Keywords: aspheric compound eyes (ACEs), micro milling, tool path optimization

1 Introduction

Artificial compound eyes are multi-aperture optical systems inspired by the insect visions with many specific superiorities like wide field of view (FOV), light weight and high temporal resolution, which exhibit potentially considerable potent applications in the industrial and military regions. In the near future, artificial compound eyes will be expected to serve as key components in the aspects of missile guidance, radar detection, early-warning satellite, lighting and visual imaging. Meanwhile, they may play an important role in the fields of large infrared telescope, micro-camera and fingerprint identification systems[1–2]. Therefore, over the past decade, many efforts have been devoted to investigate on compound eyes, among which structure optimization and high-precision manufacture of artificial compound eyes have been the main research hotspots in the region of optical bionics[3–4]. The common structure of compound eyes is two-dimensional (2D) on which the arrangement of lenslets is uniform, thereby resulting in a strong fluctuation of the imaging performance over the object distance and a limited FOV[5–6]. In the recent years, some scholars have done a lot of work about the structure design and fabricating methods of three dimensional (3D) artificial compound eyes, especially on spherical compound eyes[7–8]. However, there is still a large disparity in optical performance (e.g., the resolution and FOV) between the spherical optical compound eyes and the eyes of insects, which motivates us to optimize the structure of the artificial compound eyes.

The mainly available method for fabricating compound eyes is micro-nano optical manufacturing, such as photolithography, focused ion beam and laser direct writing. DUPARRÉ, et al[3], processed compound eye structure on a planar substrate by UV lithography in 2004. Then they also gained the micro-lens array on the curved surface through laser direct writing in 2007[7]. JUNG, et al[9], fabricated ommatidia using laser induced self-writing process for high-resolution compound-eye optical systems. GAO, et al[10], gained artificial analogues by soft lithography. In 2010, OH, et al[11], fabricated micro-lens array using quartz wet etching and polymer. Some researchers[12–13] also tried to adopt the LIGA-like technology and thermal imprinting to construct compound eyes. Micro-nano optical manufacturing has good performance in fabricating micro-scale optical devices, but it is also a time-consuming and high-cost processing method with uncontrollable

* Corresponding author. E-mail: chenmj@hit.edu.cn
Supported by National Natural Science Foundation of China (Grant No. 50935003), and National Numerical Control Major Projects of China (Grant No. 2013ZX04001000215)

precision and poor dimensional homogeneity which make it difficult to further improve the imaging quality of compound eyes. Furthermore, micro-nano optical manufacturing is mainly used to process the simple curved surface (sphere or cylinder)[14].

Precision machining with advantages in processing three-dimensional micro structure is a feasible way to fabricate artificial compound eyes. In 2009, LI, et al[15], fabricated 3D micro-lens array projection by the diamond machining on spherical surface. In 2010, they utilized the combination of regular diamond turning, diamond broaching slow tool servo and micro milling to machining compound-eye systems consisting of the prescribed three arrays, 3D micro prism array, the micro-lens array and the aperture array[16]. The well-known direct 3D micro machining methods can be used to directly generate true 3D microstructures or patterns by means of real tools on both planar and curved surfaces. In coordination with the injection mould, 3D micro machining can also improve the manufacturing efficiency of artificial compound eyes. Moreover, the processing accuracy is controllable with good dimensional homogeneity[17–18]. Therefore the precision machining provides a promising way to fabricate the compound eyes. However, few have been reported in literatures on fabricating compound eyes by micro milling. This paper attempts to manufacture ACEs using micro milling. In order to obtain ACEs with high imaging quality, the tool paths were optimized by analyzing the influence factors consisting of interpolation allowable error, scallop height and tool paths pattern. The tool paths were planned and machining experiments were conducted to verify them.

2 Model Construction

Spherical aberration, one of the optical aberrations, is inevitable in the spherical compound eyes affecting the imaging quality[19]. Therefore it is necessary to calibrate the spherical aberration. The aspheric structure is one of the ways to calibrate the spherical aberration. The aspheric surface of the compound eye was designed to improve the imaging quality and eliminate the imaging blind area. The structure of ACE incorporated the characteristics of hexagon honeycomb, aspheric surface and non-uniform micro-lens array[20]. Composed with hexagon ommatidia (micro-lens), the new structure was more compacted, and the non-uniform micro-lens array produced a larger FOV. The procedure of the construction includes designing the general structure, calculating the azimuth angle and focal length of each group of ommatidia, modeling and splicing the ommatidia. The spatial distribution of ommatidia is illustrated in Fig. 1.

The profile of the ommatidium is hexagon and all the apexes of the hexagons are on the same spherical surface as shown in Fig. 1(b). Azimuth angle ($\alpha_1, \alpha_2, \cdots, \alpha_n, \beta_1, \beta_2, \cdots, \beta_n$) of the ommatidium is calculated according to their geometrical relationship, and focal length ($l_{F1}, l_{F2}, \cdots, l_{Fn}$) is worked out to make every ommatidium focus on the same receiving plane. The design of aspheric surfaces for the ommatidia is of key important to calibrate the spherical aberration. The general equation describing the aspheric surface is shown as follows[21]:

$$z=\frac{y^2}{r+\sqrt{1-(1+k)r^2y^2}}+a_1y^2+a_2y^4+a_3y^6+\cdots+a_ny^{2n},\ n\in N, \tag{1}$$

where z is the axial distance from the origin of coordinate; y is the distance from the symmetry axis; k is the cone coefficient; $a_0, a_1, \cdots, a_n$ is the high order aberration coefficients; and r is the curvature radius of the vertex.

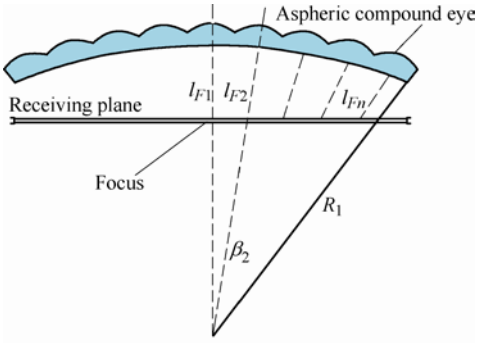

(a) Geometric scheme of azimuth angle of ommatidia

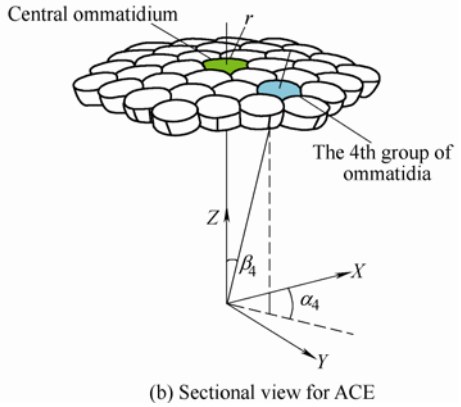

(b) Sectional view for ACE

Fig. 1. Spatial distribution of ommatidia

The aspheric model is designed by successive approximation method[22]. The procedure includes building the original spherical model, calculating conical section equation and adding the high order aberration coefficients. The third task is done with the help of ZEMAX. Here we mainly discuss the calculation of conical section equation.

The original spherical model is built according to the focal length. In order to calibrate the marginal spherical aberration, the front surface of the ommatidia must be refined into aspheric surface. The optical path from the front surface to the back one was drawn on the basis of refraction principle, as shown in Fig. 2.

The general equation of the conical section is,

$$y^2=2r_nx+bx^2, \tag{2}$$

where r_n is the spherical radius of the front surface in the original model. Taking incident point (d, H) into Eq. (2), the equation is changed into,

$$H^2 = 2r_n d + bd^2. \tag{3}$$

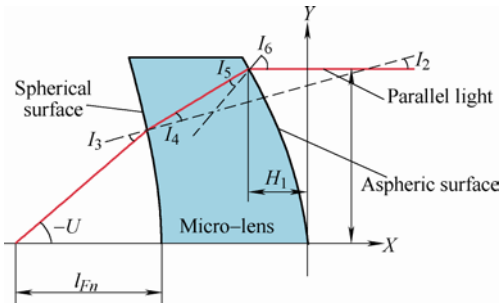

Fig. 2. Refraction path

According to the geometric relationship and refraction principle, Eq. (4) can be deduced,

$$\begin{cases} \dfrac{R_1}{\sin I_1} = \dfrac{R_1 - l_{Fn}}{\sin I_3}, \\ I_2 = I_1 - I_3, \\ I_6 - I_5 = I_2 + I_4, \\ m_0 \sin I_6 = m_1 \sin I_5, \\ m_0 \sin I_3 = m_1 \sin I_4. \end{cases} \tag{4}$$

where R_1 is the spherical radius of back surface, the default value of R_1 is 20 mm, m_0 and m_1 are the refractive index of air and microlens material, respectively, I_1, I_2, $\cdots$, I_6 are the corresponding optical angle (incidence angle, refraction angle or emergence angle).

According to Eq. (4), the incidence angle (I_6) on the conicoid can be obtained. The normal curvature (k=tanI_6) on the refraction point of conicoid can be calculated according to this equation,

$$\left.\frac{\mathrm{d}x}{\mathrm{d}y}\right|_{y=H,x=d} = \frac{H}{r_n + bd} = k. \tag{5}$$

The values of b and d can be gained from Eq. (3) and Eq. (5). The cone coefficient is k=b–1. Therefore all the coefficients of conical equation are ascertained. The high order aberration coefficients are obtained using ZEMAX. The equation of central ommatidium (No. 0) is shown as follows:

$$z = \frac{y^2}{1.406 + \sqrt{1.406^2 - (1-0.492)y^2}} - 9.916\times10^{-5} y^2 + 1.363\times10^{-3} y^4 + 1.515\times10^{-4} y^6. \tag{6}$$

The three-dimensional model is built by splicing the ommatidia according to their own azimuths. The ommatidia on the same circle are labeled as Group 1, 2, $\cdots$, 7 from inside to outside. As shown in Fig. 3, each group has 6 ommatidia except Group 1 with only one ommatidium. The ommatidia are numbered from No. 0 to No. 36 clockwise from Group 1 to Group 7. The size of ACE is 7 mm×7 mm and the aperture of the ommatidium is 1.31 mm.

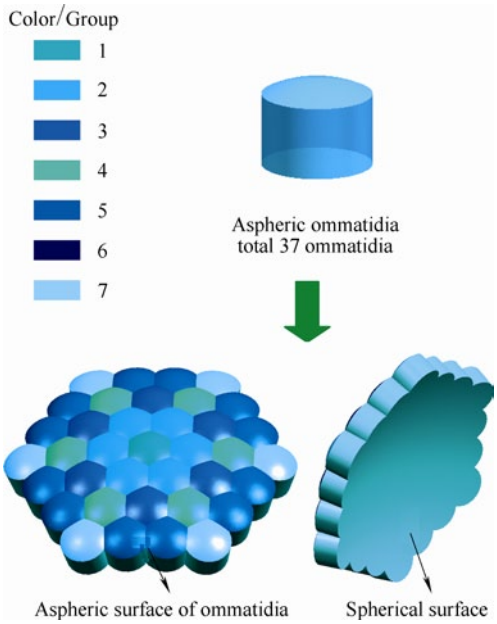

Fig. 3. Three-dimensional model of compound eyes

The imaging quality of the ACE model was checked by simulation of ray tracing[23]. It was found that the marginal spherical aberration of ACE was below 60 μm whereas that of the spherical compound eyes with the same aperture was up to 400 μm, as shown in Fig. 4. Therefore, the non-uniform ACE can calibrate the marginal spherical aberration effectively.

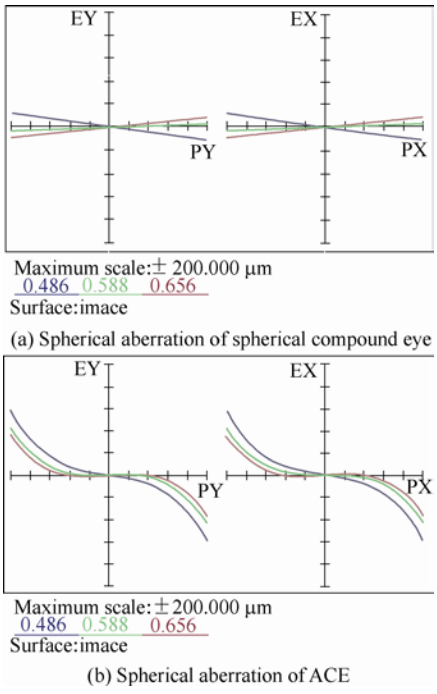

Fig. 4. Comparison of spherical aberration

3 Analysis ofInfluencing Factors on Tool Path Optimization

High precision and low surface roughness are essential to high imaging quality of optical compound eyes. This paper tries to find out how the interpolation allowable error, scallop height and tool paths pattern affect the precision of tool paths for computer numerical control (CNC) milling.

3.1 Analysis of interpolation allowable error

Interpolation allowable error is the maximum allowable deviation between the actual tool path and the ideal tool path. Choosing ball end mill to cut, the local geometrical relationship of interpolation is magnified in Fig. 5. Since the mould of the compound eye is concave, we just discuss the interpolation error in the case of concave.

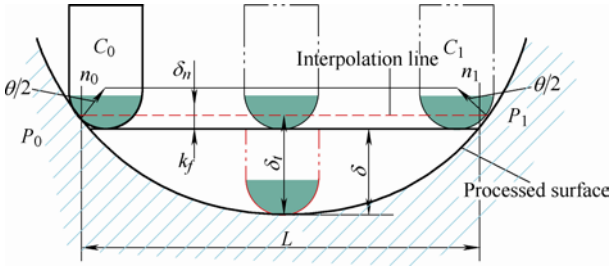

Fig. 5. Local geometrical relationship of interpolation

It is presumed that k_f is the normal curvature of the processed surface along the feed direction in the interpolation section, θ is the rotation angle of the normal vector along the interpolation linear orientation, the ball end mill moves linearly from C_0 to C_1, and the interpolation error δ is,

$$\delta = \delta_t - \delta_n, \tag{7}$$

where δ_n is the normal vector rotation error, δ_t is the linear approximation error (chord error). The expression of δ_n can be obtained according to Fig. 4,

$$\delta_n = R - R\cos\frac{\theta}{2} = 2R\sin^2\frac{\theta}{4} \leqslant \frac{1}{8}R\theta^2 = \frac{1}{8}Rk_f{}^2(\Delta s)^2, \tag{8}$$

where Δs is the arc length in interpolation section.

$$\delta_t = \frac{\Delta s}{2\sin\dfrac{\theta}{2}}\left(1-\cos\frac{\theta}{2}\right) = \frac{\Delta s}{2\cos\dfrac{\theta}{4}}\sin\frac{\theta}{4} \leqslant \frac{1}{8}\Delta s\theta = \frac{1}{8}k_f(\Delta s)^2. \tag{9}$$

From Eq. (8) and Eq. (9), $\delta_t \gg \delta_n$ is concluded.

$$\delta = \delta_t - \delta_n < \delta_t \leqslant \frac{1}{8}k_f(\Delta s)^2. \tag{10}$$

Replacing Δs with chord length L, distance between the two adjacent location points of the cutter is also called cutting length step.

$$\delta = \delta_t - \delta_n < \delta_t \leqslant \frac{1}{8}k_f L^2. \tag{11}$$

Supposing ε is the interpolation allowable error and $|\delta| < \varepsilon$, we can get the following relationship,

$$\frac{1}{8}k_f L^2 \leqslant \varepsilon, \tag{12}$$

$$L \leqslant 2\sqrt{\frac{2\varepsilon}{|k_f|}}. \tag{13}$$

According to the relationship presented in Eq. (13), it can be found that if the value of L is reasonable and meets the requirement of the interpolation allowable error, the precision of the curved surface will be guaranteed.

3.2 Analysis for scallop height

Scallop height is one of the important factors influencing surface roughness. In the finishing machining, the value of scallop height is related with the width of tool path and the radius of tool. When processing compound eyes, there is an angle between the processing surface and the cutting plane formed by parallel tool paths. The angle varies in different regions. The axle of the ball end mill tilts for good cutting performance and proper cutting speed. Taking the small segment of curved surface as a slope, the geometry relationship can be shown in Fig. 6.

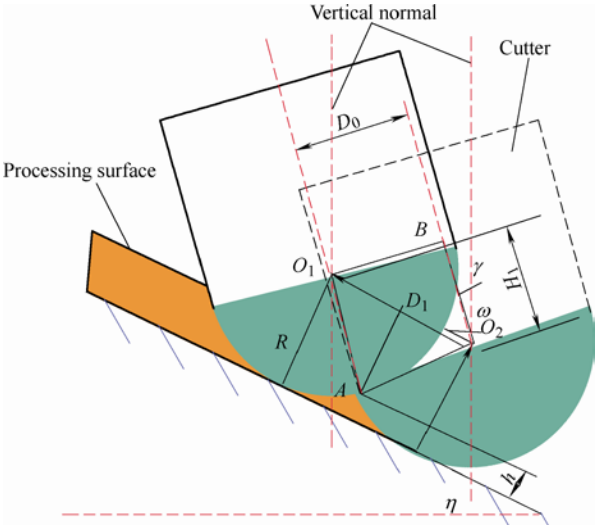

Fig. 6. Geometry relationship of slope

The following two equations are gained:

$$D_1 = \frac{D_0}{\sin(\omega-\gamma)} = \frac{D_0}{\cos(\eta+\gamma)}, \tag{14}$$

$$h = R - \sqrt{R^2 - \left(\frac{D_1}{2}\right)^2} = R - \sqrt{R^2 - \left(\frac{D_0}{2\cos(\eta+\gamma)}\right)^2}, \quad (15)$$

where D_0 is the milling width, D_1 is the width of actual tool path on the slope, η is the angle of the slope along the horizontal direction, ω is the angle of the slope along the vertical direction, γ is the angle of tool axle along the vertical direction, R is the radius of tool, h is the scallop height, H_1 is the milling depth.

Some special cases of Eq. (15) are as follows.

In the case of γ=0°, namely the tool axle is vertical, Eq. (15) changes into

$$h = R - \sqrt{R^2 - \left(\frac{D_0}{2\cos\eta}\right)^2}. \quad (16)$$

In the case of γ=0°, η=0°, namely, the tool axle is vertical and the processing surface is horizontal, Eq. (15) changes into

$$h = R - \sqrt{R^2 - \left(\frac{D_0}{2}\right)^2}. \quad (17)$$

If η, γ and D_0 are fixed, the derivation about R of Eq. (15) is

$$h' = 1 - \frac{R}{\sqrt{R^2 - \left(\frac{D_0}{2\cos(\eta+\gamma)}\right)^2}} < 0. \quad (18)$$

In these equations, if the tool axle and the slope are on the same side of the vertical normal, as shown in Fig. 6, γ is positive and negative otherwise. The following conclusions are obtained from Eq. (15), the scallop height decreases as D_0, η and γ decrease. If D_0, η and γ are fixed, the scallop height will reduce as the radius of tool rises. The slope coefficients are different in different regions of compound eye. Therefore if the tool paths for each ommatidium are planned with fixed linear approximation error and scallop height considering its geometric position, it is easy to get high surface quality in finishing machining. The tool path will be planned based on these conclusions.

3.3 Analysis of tool paths pattern

Here the different affects of circular milling and parallel milling on fabricating compound eyes are discussed. Circular milling is down milling or up milling whereas parallel milling transforms alternately between down milling and up milling if the tool processes reciprocally. The variation of the feed direction and the cutting force will affect the surface quality. Consequently, circular milling has more advantages than parallel milling in the finishing machining which requires high machining quality.

4 Scheme and Simulation of Tool Paths

4.1 Tool paths for rough machining

The rough machining was to remove the material of the blank. In this paper, the profile of compound eye was firstly processed by reciprocal-parallel milling with a machining allowance of 5 μm. The parameters of tool paths were determined according to the factors analyzed above, as shown in Table 1. The tool paths were gained, as shown in Fig. 7. The tool paths were layered and the curves on each layer were parallel.

Table 1. Parameters of tool paths for rough machining

Tool paths pattern	Milling depth	Milling width	Processing sequence
Reciprocal-parallel milling	Changeable (8–20 μm)	24 μm	Sectional priority

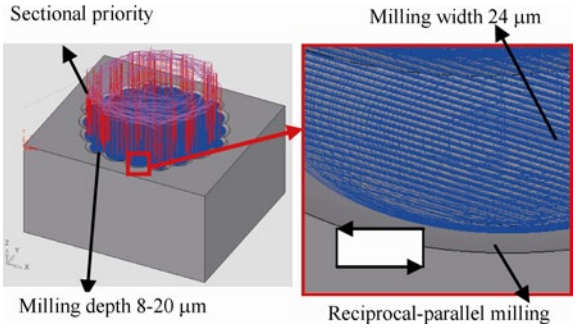

Fig. 7. Tool paths for rough machining

4.2 Tool paths for finishing machining

After rough machining, the remained material must be removed to improve the surface quality. Two schemes of tool paths for finishing machining were planned to verify the analysis result of the third part (analysis of influencing factors on tool path optimization).

(1)Scheme (I)—circular-milling for the entire ommatidia

Scheme (I) was planned to circularly mill all the ommatidia at a time. The milling width was 3 μm.The tool paths ran through all the ommatidia, as shown in Fig. 8.

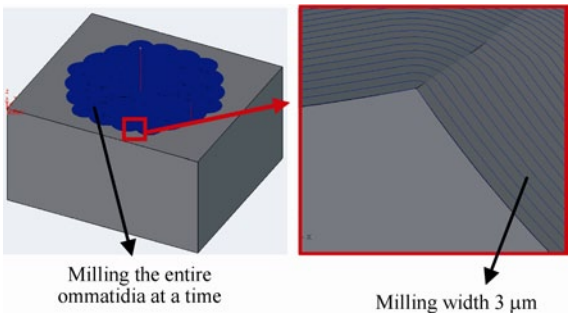

Fig. 8. Circular-milling for the whole compound eye

(2) Scheme (II)—circular- milling for each ommatidium

Scheme (II) was planned to circularly mill each ommatidium individually according to its geometric position. The tool path for each ommatidium was different. Three kinds of tool paths patterns were planned, parallel layered milling, circular layered milling with changeable milling depth, and circular layered milling with fixed milling depth. However, there might be some small protuberances remained in the center of the ommatidium. A special tool path was added manually to wipe them out, as shown in Fig. 9.

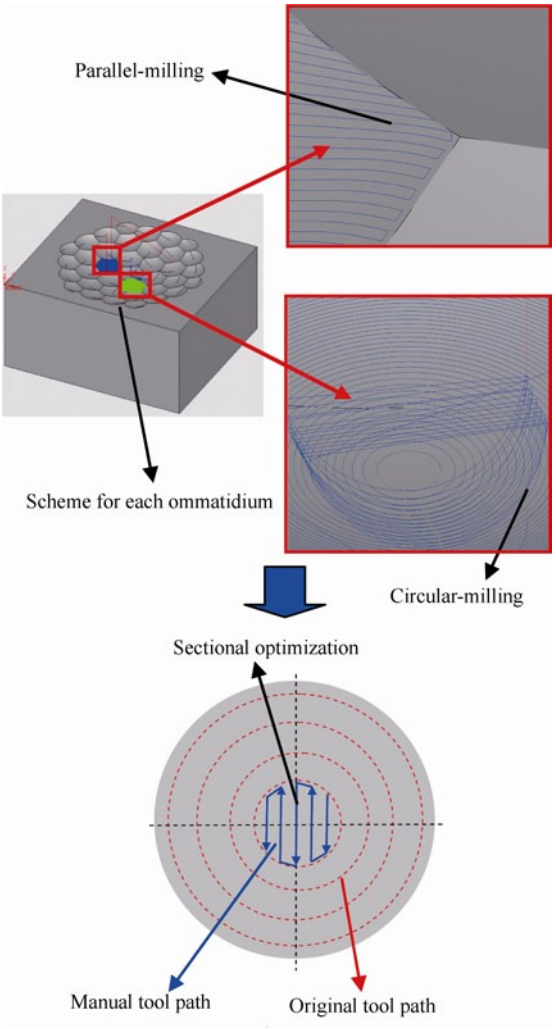

Fig. 9. Circular-milling for each ommatidium

4.3 Simulation of tool paths

The simulation was carried out using Cimatron E to verify the tool paths. As shown in Fig. 10, the models of compound eyes were processed correctly in the simulation. After the simulation, the tool paths could be changed into G codes through post-processing. The G codes could be used directly to process the compound eyes on the precision CNC micro milling machine tool.

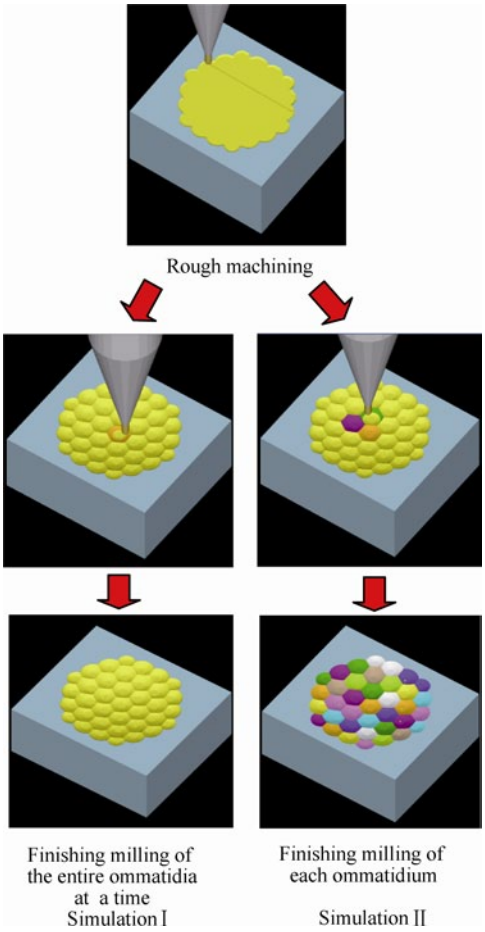

Fig. 10. Simulation procedure

5 Machining Experiments

5.1 Experimental condition

The main device for experiments is the miniature precision five-axis milling machine tool designed by our group, as shown in Fig. 11.

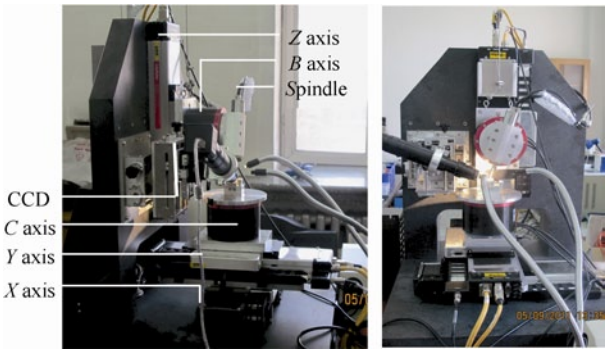

Fig. 11. Miniature precision five-axis milling machine tool

The resolution of grating in linear axis is 0.1 μm and the position accuracy is 0.5 μm in the scale of 7 mm×7 mm. The highest rotating speed of spindle is 80 kr/min. The blank is an organic-glass rectangular block with the dimension of 20 mm×20 mm×10 mm. The tool is a micro double-edge ball-end milling cutter produced by NS Company in Japan (No. MSB230).

5.2 Experiments

According to the tool paths planned above, two compound eyes were processed. One was called "entire-circular-milling prototype workpiece" (Sample I), and the other was called "single-circular-milling prototype workpiece" (Sample II). The radius of milling cutter of 50μm and the tilt angle (θ) of 20° were selected to fabricate the whole-circular-milling prototype workpiece. Reciprocal-parallel milling was adopted in the rough machining, and Scheme (I) was applied to the finishing machining. To process the single-circular-milling prototype workpiece, the radius of 200 μm for the milling cutter and the tilt angle of 20° were adopted. Specially, tool path pattern for No. 1 ommatidium was parallel-milling for further comparison with circular-milling. Tool path pattern for the rest was circular-milling. The corresponding machining parameters for the two workpieces were shown in Tables 2–4 respectively.

Table 2. Machining parameters for whole-circular -milling prototype workpiece

Process type	Tool path pattern	Milling depth a_p/μm	Milling width a_e/μm	Spindle speed n/(r • min^{-1})	Feed rate per tooth f_z/(μm • z^{-1})	Allowance for machining A/μm
Rough	Parallel-milling	8	10	30 000	1	3
Finishing	Circular-milling	3	3	40 000	0.8	0.1

Table 3. Rough machining parameters for single-circular -milling prototype workpiece

Process type	Tool path pattern	Milling depth a_p/μm	Milling width a_e/μm	Spindle speed n/(r • min^{-1})	Feed rate per tooth f_z/(μm • z^{-1})	Allowance for machining A/μm
Rough	Parallel-milling	20	24	40 000	1.5	5

Table 4. Finishing machining parameters for single-circular-milling prototype workpiece

Ommatidium No.	Tool path pattern	Milling depth	Distance between adjacent cutting layers a_p/μm	Scallop height limit H/μm	Milling width a_e/μm	Feed rate per tooth f_z/(μm • z^{-1})	Spindle speed n/(r • min^{-1})
0	Circular-milling	Changeable	1	0.01	—		
1	Parallel-milling	Fixed	—	—	1		
2	Circular-milling	Changeable	2		—		
3	Circular-milling	Changeable	3	0.1	—		
4	Circular-milling	Changeable	4		—		
5	Circular-milling	Changeable	5		—	1	60 000
6	Circular-milling	Fixed	2	—	—		
7	Circular-milling	Fixed	3	—	—		
8	Circular-milling	Fixed	4	—	—		
9	Circular-milling	Fixed	5	—	—		
The rest	Circular-milling	Changeable	3	0.1	—		

The pictures of the two prototype workpieces were shown in Fig. 12. The tool marks could be seen clearly on the surface of entire-circular-milling prototype workpiece because of the unreasonable cutting parameters and tool path pattern. In contrast, the latter had clear hexagon-profile ommatidia with few cutter marks. Consequently, it had verified that the surface quality of the ACE obtained by Scheme (II) was better than that of the ACE obtained by Scheme (I).

5.3 Measurement results

The roughness of the single-circular-milling prototype workpiece was measured by the roughness profilometer of Taylor Hobson. The roughness curve of No. 0 ommatidium was shown in Fig. 13 (R_a=0.115 μm). The roughness of other ommatidia was below 0.12 μm except that the R_a of No. 1 ommatidium is 0.48 μm. The imaging performance of ACE was observed by super depth field microscope. As shown in Fig. 14, the ommatidium of the ACE could image the same object individually. The images formed by No. 1 ommatidium labeled by red circles were distorted, because the adopted tool path pattern was parallel-milling and the value of roughness was higher. In a word, the tool paths had a great effect on imaging quality.

6 Conclusions

(1) The marginal spherical aberration of the ACE is below 60 μm according to the simulation of ray tracing, whereas that of the spherical compound eye with the same aperture is up to 400 μm. It indicates that the non-uniform aspheric structure can calibrate the marginal optical aberration and improve the imaging quality effectively.

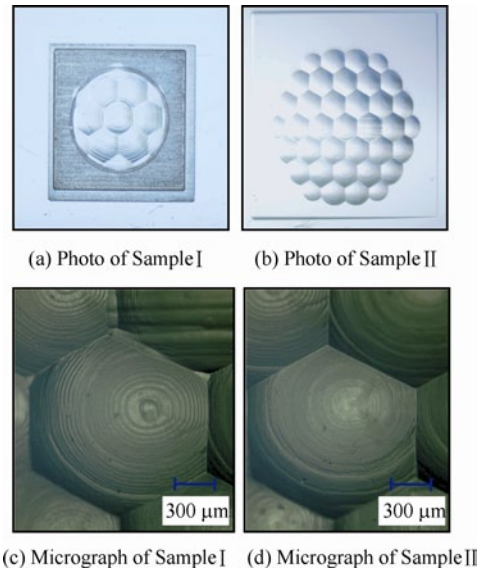

Fig. 12. Pictures of two prototype workpieces

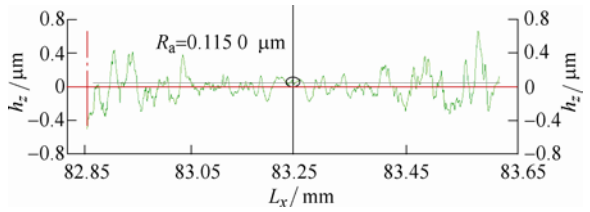

Fig. 13. Roughness curve of No. 0 ommatidium

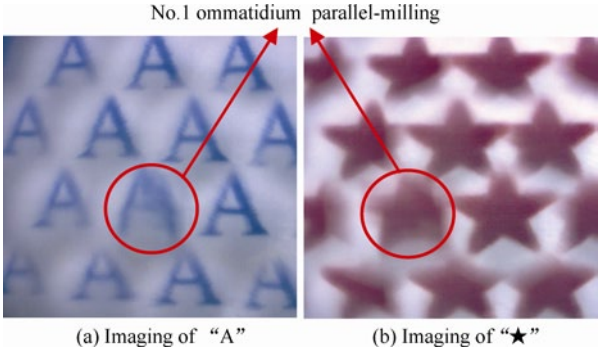

Fig. 14. Imaging of the prototype workpiece

(2) The effect of interpolation allowable error, scallop height and tool path pattern on the precision of tool paths for CNC milling show that reasonable cutting length step, changeable cutting depth and width in different regions could lead to high-precision tool paths and improve surface quality of the compound eyes.

(3) The circular milling for each ommatidium is shown to be much better than circular milling for the entire compound eye on the basis of the planned tool paths of rough and finish machining, which is verified by simulation and experiment.

(4) The surface roughness (R_a) of the compound eyes is below 0.12 μm, and the machined models have the same imaging function as the compound eyes. The machining experiments prove that micro milling is a feasible way to fabricate compound eyes with high surface quality and good imaging performance. Moreover, micro milling is flexible and controllable in processing compound eyes on free-form surface.

References

[1] JEONG K H, KIM J, LEE L P. Biologically inspired artificial compound eyes[J]. *Science*, 2006, 312 (5773): 557–561.

[2] DUPARRE J, SCHREIBER P, VOLKEL R. Theoretical analysis of an artificial superposition compound eye for application in ultra flat digital image acquisition devices[C]//*Proceedings of SPIE. Optical Design and Engineering*, St. Etienne, France, September 30, 2003, Bellingham, 2003, 5249: 408–418.

[3] WIPPERMANN F, DUPARRE J, SCHREIBER P. Applications of chirped microlens arrays for aberration compensation and improved system integration[C]//*Proceedings of SPIE. Novel Optical Systems Design and Optimization IX*, San Diego, USA, August 13, 2006, 6289: 628915-1-9.

[4] HAMANAKA K, KOSHI H. An artificial compound eye using a microlens array and its application to scale-invariant processing[J]. *Optical Review*, 1996, 3(4): 264–268.

[5] DUPARRE J, WIPPERMANN F, DANNBERG P, et al. Chirped arrays of refractive ellipsoidal micro-lenses for aberration correction under oblique incidence[J]. *Optics Express*, 2005, 13(26): 10 539–10 551.

[6] WIPPERMANN F, DUPARRE J, SCHREIBER P, et al. Design and fabrication of a chirped array of refractive ellipsoidal micro-lenses for an apposition eye camera objective[C]//*Proceedings of SPIE. Optical Design and Engineering II*, Jena, Germany, September 12, 2005, 5962: 59622C-1-11.

[7] DUPARRE J, RADTKE D, TUNNERMANN A. Spherical artificial compound eye captures real images[C]//*Proceedings of SPIE. MOEMS and Miniaturized Systems VI*, San Jose, USA, January 20, 2007, 6466: 64660K-1-9.

[8] RADTKE D, DUPARRE J, ZEITNER U D, et al. Laser lithographic fabrication and characterization of a spherical artificial compound eye[J]. *Optics Express*. 2007, 15 (6): 3067–3077.

[9] JUNG H, JEONG K H. Microfabricated ommatidia using a laser induced self-writing process for high resolution artificial compound eye optical systems[J]. *Optics Express*. 2009, 17(17): 14 761–14 766.

[10] GAO X F, YAN X, YAO X, et al. The dry-style antifogging properties of mosquito compound eyes and artificial analogues prepared by soft lithography[J]. *Advanced Materials*, 2007, 19(17): 2213–2217.

[11] OH H, KIM G, SEO H, et al. Fabrication of micro-lens array using quartz wet etching and polymer[J]. *Sensors and Actuators A: Physical*, 2010, 164(1–2): 161–167.

[12] LIU K H, CHEN M F, PAN C T, et al. Fabrication of various dimensions of high fill-factor micro-lens arrays for OLED package[J]. *Sensors and Actuators A: Physical*, 2010, 159(1): 126–134.

[13] OH S S, CHOI C G, KIM Y S. Fabrication of micro-lens arrays with moth-eye antireflective nanostructures using thermal imprinting process[J]. *Microelectronic Engineering*, 2010, 87(11): 2328–2331.

[14] DUPARRE J, DANNBERG P, SCHRIEBER P. Artificial apposition compound eye fabricated by micro-optics technology[J]. *Applied Optics.*, 2004, 43(22): 4303–4310.

[15] LI L, YI A Y. Microfabrication on a curved surface using 3D microlens array projection[J]. *Journal of Micromechanics and Microengineering*, 2009, 19 (10): 1–8.

[16] LI L, YI A Y. Development of a 3D artificial compound eye[J]. *Optics Express*, 2010, 18(17): 18 125–18 137.

[17] KANG H J, AHN S H. Fabrication and characterization of microparts by mechanical micro machining: precision and cost estimation[J]. *Proceedings of the Institution of Mechanical Engineers, Part B: Journal Engineering Manufacture*, 2007, 221(2):

231–240.
[18] BANG Y B, LEE K M. 5-axis micro milling machine for machining micro parts[J]. *The International Journal of Advanced Manufacturing Technology*, 2005, 25 (9–10): 888–894.
[19] BONNEFOIS A M, GILBERT M, THRO P Y. Thermal lensing and spherical aberration in high-power transversally pumped laser rods[J]. *Optics Communications*, 2006, 259(1): 223–235.
[20] HORISAKI R, KAGAWA K, NAKAOL Y. Irregular lens arrangement design to improve imaging performance of compound-eye imaging systems[J]. *Applied Physics Express*, 2010, 3(2): 022501-022501-3.
[21] GARZA-RIVERA A, RENARO-CARRILLO F J. Design of artificial apposition compound eye with cylindrical micro-doublets[J]. *Optics Review*, 2011, 18(1): 184–186.
[22] CHEN M J, CHU X, WU C Y, et al. Research on structural design and optimization of artificial optical compound eye[J]. *Materials Science Forum*, 2012, 697–698: 817–821.
[23] GARCIA-LIEVANOS O, VAZQUEZ-MONTIEL S, HERNANDEZ-CRUZ J A. Optical design with aspheric surfaces and exact ray tracing: An analytic method[C]//*Proceedings of SPIE. International Optical Design Conference*, Vancouver, Canada, June 04, 2006, 6342: 63422H-1-8.

Biographical notes

CHEN Mingjun, born in 1971, is currently a professor at *Harbin Institute of Technology*, *China*. He received his PhD degree from *Harbin Institute of Technology*, *China*, in 2001. His research interests include ultra-precision machining and micro-nano manufacturing technology.
Tel: +86-451-86403252; E-mail: chenmj@hit.edu.cn

XIAO Yong, born in 1988, is currently a PhD candidate at *Mechanical Manufacturing and Automation*, *Harbin Institute of Technology*, *China*. He received his master degree of engineering in *Harbin Institute of Technology*, *China*, in 2012. His research interests include ultra-precision machining.
Tel: +86-451-86403252; E-mail: xydream@126.com

TIAN Wenlan, born in 1987, is currently an engineer at *Changchun FAW-Volkswagen*, *China*. She received her master degree of engineering from *Harbin Institute of Technology*, *China*, in 2012.
E-mail: tianwenlanjx0601@126.com

WU Chunya, born in 1982, is a lecturer at *Harbin Institute of Technology*, *China*. She received her master degree of engineering in *Harbin University of Science and Technology*, *China*, in 2008. Her research interests include ultra-precision machining and micro-nano manufacturing technology.
E-mail: wuchuya1982@163.com

CHU Xin, born in 1982, is currently an engineer at *Southwest China Research Institute of Electronic Equipment*, *China*. He received his master degree of engineering in *Harbin Institute of Technology*, *China*, in 2011.
E-mail: chuxinemail@gmail.com